ELSEVIER

Journal of Power Sources 62 (1996) 167–174

JOURNAL OF POWER SOURCES

# Modelling of temperature distribution in a solid polymer electrolyte fuel cell stack

G. Maggio [a], V. Recupero [a], C. Mantegazza [b]

[a] *Istituto CNR-TAE, via Salita S. Lucia sopra Contesse 39, 98126 Santa Lucia, Messina, Italy*

[b] *De Nora Permelec SpA, via Bistolfi 35, 20134 Milan, Italy*

Received 8 January 1996; revised 15 May 1996; accepted 24 May 1996

**Abstract**

The production of electricity in a fuel cell system is associated with the production of an equivalent amount of thermal energy, both for large size power plants and for transportation applications. The heat released by the cells must be removed by a cooling system, characterized by its small size and weight, which must be able to assure uniform work conditions and reduce performance losses. Based upon realistic assumptions, a mathematical model has been developed to determine the temperature and current density distribution in a solid polymer electrolyte fuel cell (SPEFC) stack as a function of operating conditions and stack geometry. The model represents a useful tool to identify operating conditions, such as to have an optimal longitudinal and axial temperature profile, so allowing the design of cooling system and bipolar plates. In this paper, the model has been applied to determine the temperature profile of an experimental SPEFC stack. The model is validated by comparing model results with experimental measurements; simulated and experimental results agree satisfactorily.

*Keywords:* Solid polymer electrolyte fuel cells; Stack designs; Cooling systems; Temperature profile; Modelling

## 1. Introduction

A fuel cell stack usually consists of a number of single cells connected in electrical series. Each cell, whose basic elements are a matrix containing electrolyte and porous electrodes (anode and cathode), is connected to the adjacent one through bipolar plates ribbed with channels that allow the flow of gases. Thus, the bipolar plates are gas and current collectors, and they provide the separation between the fuel and oxidant flows in adjacent cells.

Since the electrical energy produced by the cells involves a corresponding amount of thermal energy, it is necessary to study an appropriate cooling system that can remove this heat and maintain the working temperature at a constant value. In fact, high temperature gradients affect the cell performance [1]. In particular, in solid polymer electrolyte fuel cells (SPEFCs), temperature gradients cause problems with water management and electrochemical reactions, then reducing the cell lifetime [2]. Heat removal is generally accomplished through the use of cooling plates, which are usually placed in every repeating unit of a given number of working plates. It is evident that different cooling fluids (air, oil, water, etc.) and geometric configurations (channels, tubes, solid surfaces, etc.) with sizes, shapes and materials as variables can be proposed for an efficient cooling system. Often this choice is dictated by practical and economic requirements; a simplified cooling system is preferable in comparison with solutions which further increase the system complexity and management.

Even if experimental analyses and/or theoretical treatments of these problems have been carried out by other research groups, see Refs. [3–6], only few literature works [7,8] are devoted to the application of these studies to the case of SPEFC. In fact, this type of fuel cell has been extensively studied mainly from the experimental viewpoint, while the theoretical studies concerned exclusively micromodels for the single cell and its components [9–11].

This paper presents a three-dimensional mathematical model applied to study the current and temperature distribution of an SPEFC stack, whose cooling system is represented by U-tubes supported by each working plate; the cooling fluid is water. The model has been applied to verify the results of an experimental stack built by De Nora Permelec SpA (DNP) Milan, Italy [12]. For this purpose, the simulation model has been studied appropriately to comply with the technical characteristics of the DNP stack. The results obtained by the model are in good agreement with experimental measurements and demonstrate the validation of the model calculations. A sensitivity analysis of the calculated temperature profiles as a function of the operating conditions and the


*PII* S0378-7753(96)02433-0

cooling system geometry allowed the optimization of the stack design. In particular, the cooling system warrants an average temperature close to the typical values for this kind of fuel cell (70–75 °C) and a uniform temperature profile in the stack.

## 2. Experimental

An SPEFC stack equipped with temperature and pressure probes was set up to allow monitoring of the stack operating parameters. Temperature measuring devices (*K* thermocouples) were also inserted in the core of each bipolar plate to control the temperature at the centre of the active cell area. An aluminium cooling plate, coupled with ribbed graphite current collectors, constituted the bipolar plate. Fifteen cells were assembled in one unit in a standard filter-press configuration by means of tie bolts, in order to avoid gas leakage and to ensure proper electrical contact. Humidification of the reactant gases was controlled by the use of external humidifiers allowing gas saturation at the prefixed temperature and flow rates. Nafion® 117 membranes and DNP electrodes, with 1 mg/cm$^2$ Pt loading, were used as the active components in each cell.

A schematic of the SPEFC stack is given in Fig. 1, where the repeating section of the stack — cooling plate, anodic current collector, anode, membrane, cathode and cathodic current collector — constitutes the elementary cell.

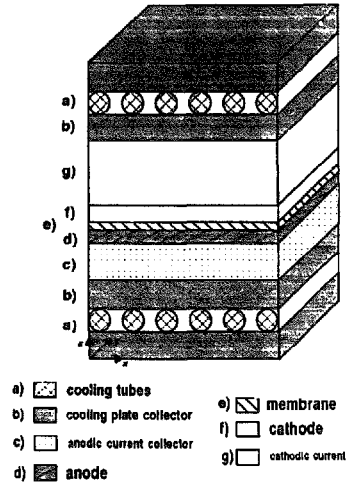


Fig. 1. Schematic view of the elementary unit of the SPEFC stack for the temperature distribution three-dimensional model.

## 3. Modelling development

To describe the distribution of current density and temperature in an SPEFC stack through a simulation model some assumptions have been made to simplify the mathematical treatment. All the assumptions, even if they do not claim to have a general validity, have been conceived so that they are coherent with the case considered and result in a realistic and appropriate description of the examined problem. The main assumptions are summarized as follows: (i) to simulate the U-tubes, the cooling system has been considered as a sequence of separate tubes of a cooling plate with water flow in alternating direction and perpendicular to the air flow; (ii) the pressure drop (using relationships reported in literature [13,14], a value of 841 Pa has been evaluated) and the effects associated with the curvature of the U-tubes have been neglected (except for some boundary conditions on the water temperature introduced to simulate the continuity between adjacent tubes); (iii) the edges of the stack operate adiabatically; (iv) the effective thermal conductivities of the plates in the air flow direction, and in the direction perpendicular to the air flow, are considered to be equal, while the thermal conductivity of the cooling tubes is considered negligible; (v) stack symmetry allows us to consider only the working plates between two different cooling plates to evaluate current and temperature distribution; and (vi) temperature gradients in the flow direction of the fuel are assumed to be negligible, i.e. the fuel heat capacity is much less than the oxidant heat capacity.

Based on these assumptions, the general equations describing the energetic balances relative to the cooling plate, the working plates, the cooling water and the process air are given by:

(i) cooling plate

$$t^{A}k_x^{A}\frac{\partial^2 T}{\partial x^2}+t^{A}k_y^{A}\frac{\partial^2 T}{\partial y^2}+k_z^{A,U}\frac{\partial T}{\partial z}\bigg|_{z+t^{A}}-k_z^{A,L}\frac{\partial T}{\partial z}\bigg|_{z}$$
$$\pm\frac{C_w m_w}{P_w}\frac{\partial T_w}{\partial x}=0 \qquad (1)$$

(ii) working plate:

$$t^{B}k_x^{B}\frac{\partial^2 T}{\partial x^2}+t^{B}k_y^{B}\frac{\partial^2 T}{\partial y^2}+k_z^{B,U}\frac{\partial T}{\partial z}\bigg|_{z+t^{B}}-k_z^{B,L}\frac{\partial T}{\partial z}\bigg|_{z}$$
$$-\frac{C_p m_p}{P_p}\frac{\partial T_p}{\partial y}=-(V^*-V)I \qquad (2)$$

(iii) cooling wate:

$$\frac{\partial T_w}{\partial x}=\pm\frac{h_w S_w}{m_w C_w}(T_w-T) \qquad (3)$$

(iv) process air

$$\frac{\partial T_p}{\partial y}=\frac{h_p S_p}{m_p C_p}(T-T_p) \qquad (4)$$

with the boundary conditions

$$\left.\frac{\partial T}{\partial y}\right|_{y=0}=0, \quad \left.\frac{\partial T}{\partial y}\right|_{y=L_y}=0 \tag{5a, b}$$

(adiabatic conditions)

$$\left.\frac{\partial T}{\partial x}\right|_{x=0}=0, \quad \left.\frac{\partial T}{\partial x}\right|_{x=L_x}=0 \tag{5c, d}$$

(adiabatic conditions)

$$T|_{z=0}=T|_{z=L_z} \tag{6}$$

(symmetric condition)

$$T_w|_{x=0,\,y=0}=T_{w,in} \tag{7}$$

$$T_w|_{x=L_x,\,y=jL_y/NC}=T_w|_{x=0,\,y=(j-1)L_y/NC} \tag{8a}$$

$1 \le j \le NC$ $j$ odd

$$T_w|_{x=0,\,y=jL_y/NC}=T_w|_{x=0,\,y=(j-1)L_y/NC} \tag{8b}$$

$1 \le j \le NC$ $j$ even

$$T_p|_{y=0}=T_{p,in} \tag{9}$$

where

$$t^{A}=t_{ct}+2t_{cc}^{A}$$

and

$$t^{B}=t_a+t_c+t_m+t_{cc,a}+t_{cc,c}+t_{cc}^{B}/2$$

are the total thicknesses of the cooling and working plate, respectively; $k$ is the effective thermal conductivity, $C$ is the heat capacity, $m$ is the mass flow and $h$ is the heat-transfer coefficient (for the other definitions the reader can refer to Section 6)

The 'plus-or-minus' terms appearing in Eqs. (1) and (3) take into account the alternating direction of the water in the U-tubes; in fact, in accordance with assumption (i) in this Section, the water flows perpendicularly to the air, going from left-side to right-side of the plates in odd tubes (sign −) and in the opposite direction in even tubes (sign +). The boundary conditions (8a) and (8b) are also valid for odd and even tubes, respectively ($NC$ is the number of cooling tubes).

The procedure used to solve these equations is based on a finite-difference method that subdivides each plate in a number of grids, which are each small enough so that temperature and concentrations variations may be neglected. Once the average current density is specified, the model calculates the voltage of each working plate. This calculation utilizes general literature relationships [15], opportunely adapted to the SPEFC, through empirical correlations that give the different overpotential losses (activation, diffusional, ohmic) as a function of the electrode characteristics.

The current density distribution on the working plates is determined as a function of the local (on the grids) reactant compositions. A solution that satisfies the input specifications (average current density, reactant utilizations and flow rates, etc.) is obtained when the differences between the local values ($I_{k,i,j}$) and an initial approximation ($I0_{k,i,j}$) of the current density are within a given tolerance:

$$\left|\frac{I_{k,i,j}-I0_{k,i,j}}{I_{k,i,j}+I0_{k,i,j}}\right| \le 0.001$$

Then, the Eqs. (1)–(4), with the boundary conditions (5)–(9), are solved to determine the temperature distributions for the cooling plate, working plates, cooling water and process air. The procedure is iterative: the final temperature distribution is obtained when the differences between the values of temperature calculated for an iteration loop and those of the previous loop (an initial approximation is used for the first loop) are lower than a specified tolerance, in accordance with the following criterion of convergence:

$$\left|\frac{T_{k,i,j}-T0_{k,i,j}}{T_{k,i,j}+T0_{k,i,j}}\right| \le 0.002$$

The finite-difference method replaces the differential Eqs. (1)–(4) with algebraic equations, substituting the derivatives with local differences evaluated in the grid points. By using the indices $i, j, k$ to denote the subdivisions along $x$-, $y$- and $z$-axes, which respectively represent the direction perpendicular to the air flow, the process air direction, and the stack (axial) direction, the finite-difference equations are:

(i) cooling plate ($k=1$)

$$\begin{aligned}&-A_1T_{k,i,j-1}+B_1T_{k,i,j}-A_1T_{k,i,j+1}-C_1^{a}T_{k+1,i,j}\\&-C_1^{c}T_{NK+1,i,j}+D_1(T_{w,i,j}-T_{w,i,j})\\&-E_1(T_{k,i-1,j}+T_{k,i+1,j})=0\end{aligned} \tag{10}$$

(ii) working plates ($2 \le k \le NK+1$)

$$\begin{aligned}&-A_2T_{k,i,j-1}+B_2T_{k,i,j}-A_2T_{k,i,j+1}-B_3T_{k-1,i,j}\\&-B_4T_{k+1,i,j}+D_2(T_{pa-1,i,j}-T_{pa-1,i,j-1})\\&-E_2(T_{k,i-1,j}+T_{k,i+1,j})=\Omega_{k,i,j}\end{aligned} \tag{11}$$

(iii) cooling water

$$T_{w,i,j}=T_{w,i,j}+(T_{1,i,j}-T_{w,i,j})[1-\exp(-\Phi_{w,i,j})] \tag{12}$$

(iv) process air ($2 \le k \le NK+1$)

$$\begin{aligned}T_{pa,i,j}=&T_{pa,i,j-1}+(T_{k+1,i,j}-T_{pa,i,j-1})\\&\times[1-\exp(-\Phi_{pa,i,j})]\end{aligned} \tag{13}$$

where $T_{k,i,j}$, $T_{w,i,j}$ and $T_{pa,i,j}$, with $1 \le k \le NK+1$, $1 \le i \le NX$ and $1 \le j \le NY$ represent the temperatures of the plates ($k=1$ for cooling plate), of the cooling water and of the process air in the grid points, $NK$ being the number of cells between two different cooling plates and $NX$, $NY$ the number of subdivisions along $x$ and $y$, respectively, and

$$T_{w,i,j}=\begin{cases}T_{w,i-1,j} & \text{for } j \text{ odd}\\ T_{w,i+1,j} & \text{for } j \text{ even}\end{cases}$$

The above coefficients are defined as follows:

Table 1
Coefficients for the finite-difference Eq. (11)

| Coefficients | $k=2$, if $NK=1$ | $k=2$, if $NK>1$ | $2<k\leq NK$ | $k=NK+1$ |
|---|---|---|---|---|
| $B_2$ | $C_1^{\,a}+C_1^{\,c}+E_4$ | $C_1^{\,a}+C_2+E_4$ | $2C_2+2E_4$ | $C_1^{\,c}+C_2+E_4$ |
| $B_3$ | $C_1^{\,a}+C_1^{c}$ | $C_1^{\,a}$ | $C_2$ | $C_2$ |
| $B_4$ | 0 | $C_2$ | $C_2$ | 0 |

When $k=NK+1$ the term $B_4T_{k+1,i,j}$ is replaced with $C_1^{c}T_{1,i,j}$.

$$A_1=\frac{k_y^{A}f^{A}}{\Delta y^2} \tag{14a}$$

$$A_2=\frac{k_y^{B}f^{B}}{\Delta y^2} \tag{14b}$$

$$B_1=C_1^{a}+C_1^{c}+E_3 \tag{15}$$

$$C_1^{a}=\frac{k_z^{A,U}}{\Delta z^{A,U}} \tag{16a}$$

$$C_1^{c}=\frac{k_z^{A,L}}{\Delta z^{A,L}} \tag{16b}$$

$$C_2=\frac{k_z^{B,L}}{\Delta z^{B,L}}=\frac{k_z^{B,U}}{\Delta z^{B,U}} \tag{16c}$$

$$D_1=\frac{C_w m_w}{P_w \Delta x} \tag{17a}$$

$$D_2=\frac{C_p m_p}{P_p Dy} \tag{17b}$$

$$E_1=\frac{k_x^{A}f^{A}}{\Delta x^2} \tag{18a}$$

$$E_2=\frac{k_x^{B}f^{B}}{\Delta x^2} \tag{18b}$$

$$E_3=2A_1+2E_1 \tag{18c}$$

$$E_4=2A_2+2E_2 \tag{18d}$$

$$\Omega_{k,i,j}=(V_k^{*}-V_{k,i,j})I_{k,i,j} \tag{19}$$

$$\Phi_{w_{i,j}}=\frac{h_{w_{i,j}}S_w}{m_w C_w}\Delta x \tag{20a}$$

$$\Phi_{p_{k,i,j}}=\frac{h_{p_{k,i,j}}S_p}{m_p C_p}\Delta y \tag{20b}$$

The coefficients $B_2$, $B_3$ and $B_4$, which appear in Eq. (11) for a generic working plate ($2\leq k\leq NK+1$), are listed in Table 1. They depend on the thermal conductivities of adjacent plates, and therefore vary with the location of the considered plate. In fact, for the first and last working plates ($k=2$ and $k=NK+1$), the conductivity between the cooling plate and the anodic ($C_1^{a}$) or cathodic section of the working plate ($C_1^{c}$) must be considered. For the other working plates ($2\leq k\leq NK$), however, only the conductivities between working plates ($C_2$) come into play.

The boundary conditions (5)–(9) become

$$T_{k,i,0}=T_{k,i,1} \tag{21a}$$

$$T_{k,i,NY+1}=T_{k,i,NY} \tag{21b}$$

$$T_{k,0,j}=T_{k,1,j} \tag{21c}$$

$$T_{k,NY+1,j}=T_{k,NX,j} \tag{21d}$$

$$T_{NK+2,i,j}=T_{NK+1,i,j} \tag{22}$$

$$T_{w0,i}=T_{w,in} \tag{23}$$

$$T_{w0,j}=T_{w1,j-1} \quad \text{(for } j \text{ even)} \tag{24a}$$

$$T_{wNX+1,j}=T_{wNX,j-1} \quad \text{(for } j \text{ odd)} \tag{24b}$$

$$T_{pk,i,0}=T_{p,in} \tag{25}$$

By considering the number of subdivisions in the air flow direction equal to the number of cooling tubes ($1\leq j\leq NY=NC$), it has been possible to express the continuity conditions between adjacent tubes (24a) and (24b), which require that the inlet water temperature in each tube (or division) is equal to the exit water temperature of the previous tube (division).

The simultaneous solution of Eqs. (10)–(13) is complex, because the number of unknown temperatures $T_{k,i,j}$, $T_{wi,j}$ and $T_{pk,i,j}$ is equal to $NX\cdot NY\cdot(NK+1)$, which is also the number of equations to be solved. To reduce the storage of matrix coefficients and the computational time, the computer code has been arranged to solve the Eqs. (10)–(13) for a fixed subdivision $i$ (that corresponds to a slice in the direction of air flow). In practice, the three-dimensional problem can be reconsidered as a two-dimensional one, solving only $NX\cdot(NK+1)$ equations for each division $NY$, rather than $NX\cdot NY\cdot(NK+1)$ simultaneous equations. For this purpose, at the first calculation loop the thermal conductivities of the plates in the direction perpendicular to the air flow are neglected ($k_x^{A}=k_x^{B}=0$, that is $E_1=E_2=0$ in Eqs. (10) and (11)) and a first approximation of the water temperatures can be calculated from specified (experimental) inlet and outlet water temperatures in the U-tube, assuming a linear variation with the length of the tube. Beginning with the second loop, the conductivities are taken into account ($k_x^{A}=k_y^{A}$ and $k_x^{B}=k_y^{B}$ according to assumption (iv) in this Section); besides, for each division $i$, the unknown temperature of the $i-1$ divisions is replaced with the calculated value (from the previous division) and the $i+1$ temperature is replaced with the *corresponding* value calculated from the previous loop.

The effects associated with the thermal conductivities of both working and cooling plates, the conduction between adjacent plates, and the separate cooling effects of the process air and cooling water have been examined. In particular, the effective thermal conductivities of the plates have been calculated as a function of both the thickness and the conductivity of the individual elements of the plate (anodic and cathodic current collectors, anode, cathode and membrane). The possibility to consider dissymmetries between anodic and cathodic elements, in terms of thickness and thermal conductivity (different materials), has also been introduced in the model.

As regards to the direction of the reactant gas flows the model allows various choices, corresponding to different configurations (perpendicular, parallel equi-current or counter-current), that do not involve modifications of the assumption (vi) of this Section.

## 4. Results and discussion

The model has been applied to verify the distribution of temperature in an experimental SPEFC stack. The stack consists of 15 cells with a surface area of 225 $cm^2$, working at a current of 100 A. Each cell is cooled (in this case the number of working plates between two cooling plates is $NK=1$) by a U-tube with 10 passages (simulated as single tubes), that have a cylindrical geometry and an internal diameter of 6 mm; the total water flow is 0.3 $Nm^3/h$ (20 Nl/h per cell) and the inlet water temperature is 71.3 °C. The other operating conditions and geometric features of the examined stack, used by the model as input data, are listed in Table 2. The electrodes are considered to have the same characteristics as CNR-TAE electrodes [16].

The effective thermal conductivity between cooling and working plate (anodic or cathodic section), calculated by the thicknesses and the conductivities of the individual elements, is 15.7 W/(m K). This is due to the fact that no dissymmetries between anodic and cathodic elements have been considered (same thickness) and the material of the cooling plates is the same as the working plates. Besides, the working and the cooling plates effective thermal conductivities (in air or perpendicular direction) were 136.5 and 205.7 W/(m K), respectively; in particular, the last one is equal to the value relative to the cooling plate collector because the thermal conductivity of the tubes was neglected. The effective thermal conductivity between two working plates, in this case, has not been considered, since the working plate is in contact with a cooling plate both in the upper and in the lower side (Fig. 1) and there is no current collector between working plates ($t_{cc}^{B}=0$).

The value of the reversible potential and the overpotentials calculated by the model as a function of the electrode characteristics are reported in Table 3. The limiting current associated with the concentration overpotential resulted equal to 1.17 $A/cm^2$. The anodic activation overpotential is, generally, a function of the carbon monoxide concentration and can be obtained by empirical equations. In the SPEFC case, the fuel stream, going into the stack, must not contain carbon monoxide (CO acts as a catalyst poison), then we assumed the anodic activation overpotential to be zero. A first approximation of the cell voltage (590.4 mV) is calculated by the model using the values of the parameters listed in Table 3. Then, this value is revised to obtain the convergence of the calculated current densities at the prefixed average current density (444 $mA/cm^2$), resulting in a final cell voltage equal to 604.6 mV.

The model validation has been accomplished comparing the calculated average cell temperature, cell voltage and outlet water temperature with the measured values (Table 4).

Table 2
Model input data

| Parameter description | Value |
|---|---|
| Working plate size | 15 cm × 15 cm |
| Prefixed average current density | 444 $mA/cm^2$ |
| Oxygen utilization coefficient | 69.6% |
| Hydrogen utilization coefficient | 66.3% |
| Cathodic total pressure | 3.0 atm |
| Anodic total pressure | 2.5 atm |
| Number of cooling tubes | 10 |
| Fuel inlet temperature | 68 °C |
| Cathode humidification temperature | 71 °C |
| Anode humidification temperature | 70 °C |
| Inlet cooling water temperature | 71.3 °C |
| Inlet process air temperature | 80 °C |
| Total cell number | 15 |
| Finite-differences along $y$ | 12 |
| Oxidant | Air |
| Cooling tubes external diameter | 8 mm |
| Electrode thickness | 0.3 mm |
| Membrane thickness | 0.17 mm |
| Cooling plate collector thickness | 2 mm |
| Current collector thickness | 1.5 mm |
| Catalyst weight | 1 $mg/cm^2$ |
| Catalyst utilization | 30% |
| Catalyst surface area | 600 $cm^2/mg$ |
| Total water flow | 0.3 $Nm^3/h$ |
| Electrode thermal conductivity | 15.56 W/(m K) |
| Membrane thermal conductivity | 0.21 W/(m K) |
| Cooling plate collector thermal conductivity | 205.7 W/(m K) |
| Current collector thermal conductivity | 30 W/(m K) |
| Working plate density | 2.65 $g/cm^3$ |
| Cooling plate density | 2.65 $g/cm^3$ |
| Working plate heat capacity | 0.405 kcal/(kg °C) |
| Cooling plate heat capacity | 0.405 kcal/(kg °C) |

Table 3
Electrode overpotentials calculated by the model

| Parameter | Value (mV) |
|---|---|
| Reversible potential | 1169.8 |
| Cathodic activation overpotential | 472.2 |
| Anodic activation overpotential | 0.0 |
| Ohmic overpotential | 103.6 |
| Concentration overpotential | 3.6 |

Table 4
Comparison between model and experimental results

| Result | Experimental | Calculated | Difference |
|---|---|---|---|
| Average temperature (°C) | 75.3 | 74.69 | −0.81% |
| Average cell voltage (mV) | 587.8 [a] | 604.6 | +2.86% |
| | 605.1 [b] | | −0.08% |
| Outlet water temperature (°C) | 73.9 | 74.3 | +0.54% |

[a] Average voltage calculated on 15 cells.
[b] Average voltage calculated on the first 14 cells.

From Table 4 it is evident that the agreement between the simulation and the experimental results is very satisfactory. The differences between experimental and calculated values of the cell temperature and the outlet water temperature are very low (less than 1%). The difference between the average cell voltage calculated by the model and the experimental one (the experimental voltages of every individual cell are reported in Table 5) is a little higher (about 3%), but this disagreement is most likely due to the poor performances of the last cell (whose voltage is 346 mV, due to an inadequate water balance of the cell), that for its accidental occurrence was not foreseeable by the model. In fact, when the average experimental voltage is calculated on the other cells, the difference reduces to 0.5 mV (less than 0.1%).

Table 5
Experimental cell voltages

| Cell number | Cell voltage (mV) |
|---|---|
| 1 | 630 |
| 2 | 588 |
| 3 | 610 |
| 4 | 616 |
| 5 | 612 |
| 6 | 590 |
| 7 | 618 |
| 8 | 613 |
| 9 | 591 |
| 10 | 603 |
| 11 | 605 |
| 12 | 611 |
| 13 | 603 |
| 14 | 581 |
| 15 | 346 |

The calculated temperature and current density distributions are represented in Figs. 2–5. In particular, the temperature profile of the cooling water and that of the cooling plate are shown in Figs. 2 and 3, respectively; the temperature profile of the working plate and its current density are depicted in Figs. 4 and 5, respectively. In accordance with the design of the DNP experimental stack, the flows of the process gases have been considered to be parallel equi-current and their inlet side is at the back of the plates. The number of grids considered for the finite-difference method is equal to

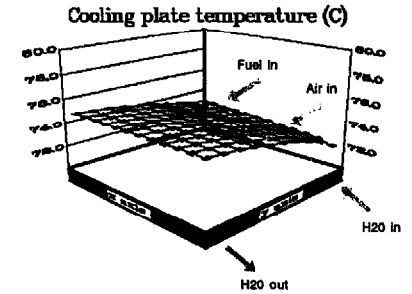


Fig. 3. Cooling plate temperature distribution for the SPEFC stack calculated by the model (input data listed in Table 2).

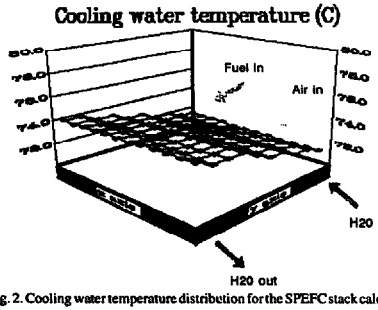


Fig. 2. Cooling water temperature distribution for the SPEFC stack calculated by the model (input data listed in Table 2).

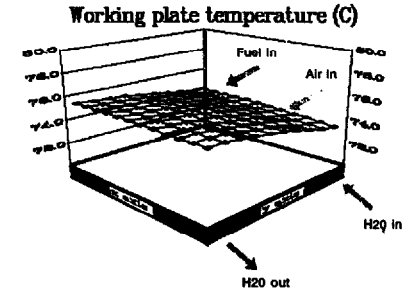


Fig. 4. Working plate temperature distribution for the SPEFC stack calculated by the model (input data listed in Table 2).

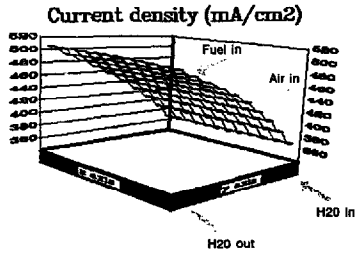


Fig. 5. Current density distribution for the SPEFC stack calculated by the model (input data listed in Table 2).

$12 \times 10$ (the second number represents the subdivisions along air flow direction and is equal to the number of cooling tubes), because this subdivision proved sufficient for an accurate solution.

The average temperatures of the cooling and working plates are 73.94 and 74.69 °C, respectively. Besides, the corresponding average temperature gradients (about 0.70 and 0.53 °C), demonstrate that a uniform temperature distribution is achieved in the stack. The average temperature of the cooling water is 72.81 °C, while that of the process air is close to the average cell temperature (74.69 °C). The average current density is 444 mA/cm$^2$, and its values range from 370 to 505 mA/cm$^2$.

## 5. Conclusions

In this paper a three-dimensional mathematical model has been proposed to study the current density and temperature profiles in an SPEFC stack. The model allows, through a sensitivity analysis, to study the influence of some geometrical (size, shape and number of the channels of the cooling plate, etc.) and working parameters (inlet temperatures and flow rates of the cooling water and air, anodic and cathodic pressure, etc.) on the stack performance.

The model validation has been successfully accomplished as evidenced by the comparison between the calculated results provided by the model and the experimental ones corresponding to an SPEFC stack with an original configuration built by De Nora Permelec SpA in Milan, Italy [12]. The stack consists of 15 cells with a surface of 225 cm$^2$ cooled by the water flowing through a U-tube (total water flow is 0.3 Nm$^3$/h at inlet temperature of 71.3 °C) and is designed for a total electrical power of 1 kW.

The average cell voltage experimentally measured for the stack is about 600 mV at 100 A, in good agreement with the value determined by the model (604.6 mV). The cell temperatures calculated by the model (average value is 74.7 °C) are in agreement with the experimental values as recorded by thermocouples placed inside the stack, with differences lower than 1% on the average values. Additionally, temperature profiles relative to the cooling plate, the process air and the cooling water have been determined by the model calculations: average values are respectively equal to 73.9, 74.7 and 72.8 °C.

The choice of appropriate operating conditions and geometrical features of the stack allowed to obtain an average temperature of the working plates (about 75 °C) close to the value required for this kind of fuel cell. A uniform distribution of the temperature in the stack has also been achieved (the gradient of temperature is less than 4 °C both in each plate and in the axial direction of the stack).

## 6. List of symbols

| | |
|---|---|
| $A_1, A_2$ | see Eqs. (14a) and (b) |
| $B_1, B_2, B_3, B_4$ | see Eq. (15) and Table 1 |
| $C$ | heat capacity, J/(kg K) |
| $C_1^a, C_1^c, C_2$ | see Eqs. (16a)–(c) |
| $D_1, D_2$ | see Eqs. (17a) and (b) |
| $E_1, E_2, E_3, E_4$ | see Eqs. (18a)–(c) |
| $F$ | Faraday constant (96487 C/g-eq.) |
| $h$ | heat-transfer coefficient, J/(s cm$^2$ K) |
| $I$ | cell current density, A/cm$^2$ |
| $k$ | effective thermal conductivity, J/(s cm K) |
| $L$ | slice length, cm |
| $m$ | mass flow, kg/s |
| $n$ | number of electrons transferred by the cell reaction (2 g eq./mol) |
| $NC$ | number of cooling tubes |
| $NK$ | number of cells between two cooling plates |
| $NX$ | subdivisions along $x$-axis |
| $NY$ | subdivisions along $y$-axis |
| $P$ | pitch of tube, cm |
| $S$ | tube perimeter, cm |
| $t$ | plate thickness, cm |
| $T$ | temperature, K |
| $V^*$ | $\Delta H/nF$, V |
| $V$ | cell voltage, V |
| $x, y, z$ | perpendicular to the process air, process air and stack (axial) direction, respectively |

*Greek symbols*

| | |
|---|---|
| $\Delta H$ | reaction enthalpy (J/mol) |
| $\Phi$ | see Eqs. (20a) and (b) |
| $\Omega$ | see Eq. (19) |

*Superscripts*

| | |
|---|---|
| A | cooling plate |
| B | working plate |
| L | lower plate |
| U | upper plate |

*Subscripts*

| | |
|---|---|
| a | anode |
| c | cathode |
| cc | current collector |
| ct | cooling tube |
| in | inlet |
| m | membrane |
| p | process air |
| w | cooling water |

## References


[1] D. Gidaspow and B.S. Baker, *AIChE J., 11* (1965) 825–837.

[2] D.P. Wilkinson, H.H. Voss and K. Prater, *J. Power Sources, 49* (1994) 117–127.

[3] H.C. Maru, C. Chi, D. Patel, D. Burns and C. Lu, *Proc. 13th IECEC, San Diego, CA, USA, Aug. 1978*, Vol. 1, pp. 723–731.

[4] C.Y. Lu and K.A. Alkasab, Manual of phosphoric acid fuel cell stack three-dimensional model and computer program, *Rep. No. CR-174722*, prepared for NASA and US Department of Energy, May 1984.

[5] G. Wilemski and T.L. Wolf, in J.R. Selman and H.C. Maru (eds.), *Symp. Electrochemical and Thermal Modeling of Battery, Fuel Cell and Photoenergy Conversion Systems*, Proc. Vol. 86-12, The Electrochemical Society, Pennington, NJ, USA, 1986.

[6] C. Rechenauer and E. Achenbach, in R.E. White, M.W. Verbrugge and J.F. Stockel (eds.), *Symp. Modeling of Batteries and Fuel Cells*, Proc. Vol. 91-10, The Electrochemical Society, Pennington, NJ, USA, 1991.

[7] M.C. Kimble and N.E. Vanderborgh, *Proc. 27th IECEC, San Diego, CA, USA, Aug. 1992*, Vol. 3, pp. 413–417.

[8] J.C. Amphlett, R.M. Baumert, R.F. Mann, B.A. Peppley, P.R. Roberge and T.J. Harris, *J. Electrochem. Soc., 142* (1995) 9–15.

[9] S.J. Ridge, R.E. White, Y. Tsou, R.N. Beaver and G.A. Eisman, *J. Electrochem. Soc., 136* (1989) 1902–1909.

[10] T.E. Springer, T.A. Zawodzinski and S. Gottesfeld, *J. Electrochem. Soc., 138* (1991) 2334–2342.

[11] D.M. Bernardi and M.W. Verbrugge, *J. Electrochem. Soc., 139* (1992) 2477–2491.

[12] *Solid Polymer Fuel Cell (SPFC) at De Nora, Informative Brochure, No. 2/95*, Apr. 1995, De Nora SpA, via Bistolfi 35, 20134-Milan.

[13] R.H. Perry and C.H. Chilton (eds.), *Chemical Engineers' Handbook*, McGraw-Hill, New York, Int. Student edn., 5th edn., Section 5, pp. 20–38.

[14] E.E. Ludwig, *Applied Process Design for Chemical and Petrochemical Plants*, Vol. 1, Gulf Publishing Co., Houston, TX, 2nd edn., 1977.

[15] D.N. Patel, H.C. Maru, M. Farooque and C.H. Ware, *J. Electrochem. Soc., 131* (1992) 2750–2756.

[16] G. Maggio and V. Recupero, Applicazione del modello di distribuzione di temperatura in uno stack al caso SPE (geometria SERE), *CNR Report No. 15/92*, prepared for De Nora Permelec, Oct. 1992.